Experimental Evaluation of the Ultimate Bending Moment of a Box Girder

J. M. Gordo and C. Guedes Soares

Unit of Marine Technology and Engineering, Technical University of Lisbon

Instituto Superior Técnico, 1049-001 Lisboa, Portugal

Abstract

The results of a four points bending test on a box girder are presented. The experiment includes initial loading cycles allowing residual stresses relief. Two indirect methods are presented for the evaluation of the residual stresses levels. The moment curvature relationship is established for a large range of curvature, the ultimate bending moment and the post buckling behavior are characterized. The distribution of stresses along the loading process is presented and the increasing lack of effectiveness of the stiffened panels is identified including an important inefficiency of the panel under tension load.

1 Introduction

The ultimate bending moment that the transverse section of a ship or a floating production and offloading platform (FPSO) can resist under overall longitudinal bending, is becoming the main criterion for reliability based design of these structures (e.g. Guedes Soares et al (1996), Sun and Guedes Soares (2003)). This move of the industry towards more accurate predictions of the strength of these structures in overall bending to resist still water and wave induced loads requires accurate and expedite methods to assess the ultimate strength.

Caldwell (1965) was the first who addressed the plastic collapse of a ship hull under overall bending although he did not allow for buckling of plate elements as pointed out by Faulkner (1965). The first attempt to incorporate the influence of the buckling collapse of some elements of the cross section was due to (Smith, 1977), who used load shortening curves of individual plate elements to calculate their contribution to the ultimate bending moment of the structure. Other methods based on this general idea were developed including the earlier ones of Billingsley (1980) and Adamchak (1984) and the more recent one of (Gordo et al, 1996).

This type of progressive collapse methods usually consider that the structural behavior of the hull girder under bending moment may be represented by the summation of the individual contributions of each longitudinal stiffened plate that is part of the cross section. The two main assumptions are that the net longitudinal force in a cross section is zero and the bending moment resulting from the external loads is equal to the first moment of the forces developed in the cross section due to the curvature of the hull girder. The first assumption requires the reevaluation of the location of the neutral axis at every incremental curvature change because of the elasto-plastic nature of the load shortening relationship for each stiffened plate element.

The ultimate moment supported by the hull is achieved after some of the elements have already collapsed, so the knowledge of shedding pattern after buckling of such elements is of great importance. Usually these methods ignore the interaction between adjacent elements thus the calculated ultimate moment may be considered as an upper limit for the maximum bending moment.

The main problem associated with such structures is the non linear behavior of the components under compression, which is a source of uncertainty on the determination of the ultimate carrying capacity of the structure, especially in a situation of overall bending where some parts are in compression and others in tension.

Because of their nature, these methods require validation by experimental results. However the number of test results available in the open literature is very limited. Two box girders representative of bridges were tested by Dowling et al (1973) and Nishihara (1984) tested seven models of scaled and simplified ship cross sections. An experiment on 1/3 scale model of a frigate was performed by Dow (1991), but this was a transversely framed ship which is not representative of most present day structures.

The predictions of the method of Gordo et al (1996) reproduced well these tests results (Gordo and Guedes Soares, 1996), but due to the limited extend of geometries involved it was decided to initiate a series of tests that would consider other geometries, covering a wider range of the different parameters that affect the ultimate carrying capacity of such structures under bending.

In this work the results of a test on a box girder representing the midship region of a ship type structure are presented and analyzed. The specimen is subjected to pure bending leading to a mode of collapse in which the upper flange failed under compressive loads.

2 Experimental details

2.1 Geometry of the specimen

The specimen is a one-meter long box girder supported by two blocks of two meters with much higher rigidity than the first. The liaison between them is bolted in order to allow the use of the supports in the future to test other models. The four points bending test is sketched in figure 1 and it allows obtaining pure constant bending throughout the whole specimen.

The central block represents the cross section of a rectangular box girder and has the major dimensions of 800mm wide and 600mm of depth. The span between the two frames of the specimen is 800mm allowing 100mm in each side for redistribution of stresses.

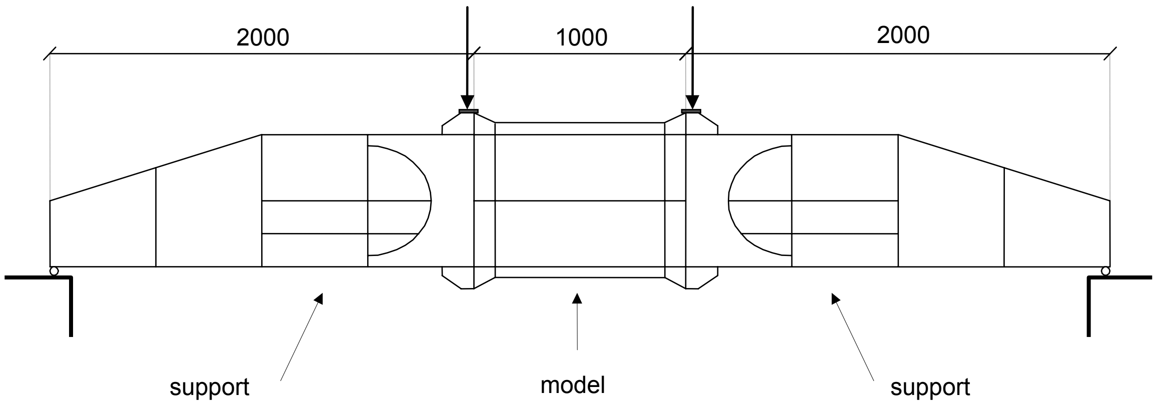

Figure 1 – Layout of the experiment

The horizontal panels, top and bottom, have three longitudinal stiffeners equally spaced (200mm) and the lateral webs have only one stiffener each. The plate is 3mm thick and the stiffeners are bars with a thickness of 4mm and 45mm of depth. This specimen was designated M3-200.

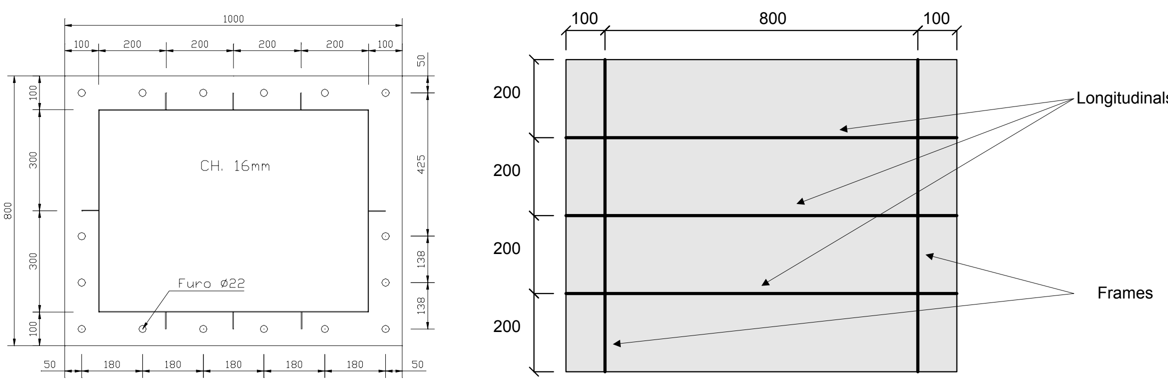

Figure 2 – Cross section (on the left) and stiffeners arrangement (on the right)

2.2 Material Properties

In the phase of specimen design it was considered that the material to be used would be mild steel with a yield stress (σ_o) of 240MPa and an elasticity modulus (E) of 210GPa. Normal ship building steel shows a marked yield followed by a yielding plateau until 8 to 10 times the yielding strain. The hardening is not very marked from this point to the ultimate strain which is normally above 20% of the initial length.

In order to obtain realistic values for the material properties tension tests were performed and the results obtained show some different values relatively to the initial assumptions.

Figures 3 and 4 are the output of those tension tests and Table 1 summarizes the main characteristics obtained with mean values of the yielding stress of 183MPa (3mm) and 310MPa (4mm) and very high ductility.

Table 1 - Mechanical characteristics of the steel used in M3-200 specimen. Tension tests.

Nominal thickness	Dimensions	Yield stress (MPa)	Maximum stress (MPa)	Elongation (%)
3	3,0x12,6	170	280	49,7
3	3,0x12,6	200	300	47,1
3	3,0x12,6	180	280	49,0
4	4,1x19,4	310	420	36,9
4	4,1x19,5	310	420	37,8
4	4,1x19,4	310	410	38,0
3	*Mean*	*183*	*287*	*48,6*
4	*Mean*	*310*	*417*	*37,6*

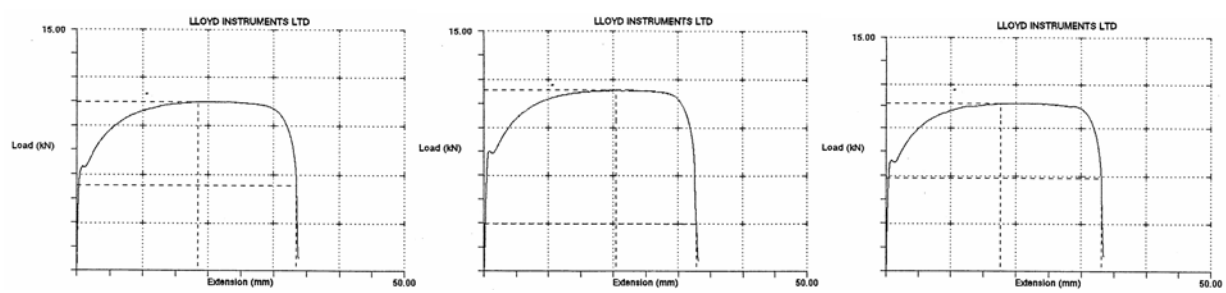

Figure 3 – Load displacement curves obtained for the tensile tests of 3mm thick steel.

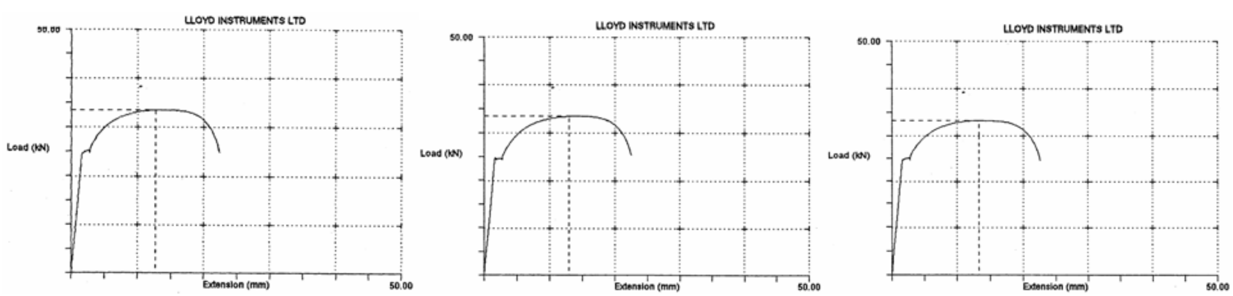

Figure 4 - Load displacement curves obtained for the tensile tests of 4mm thick steel.

3 Results of the experiment

The experiment was conducted in several cycles of loading followed by total discharges. This procedure was adopted due to the existence of residual stresses in the specimen. During the initial loading cycles the residual stresses in the panel under tension was reduced to very low values. Thus its effect on the early stage of loading is removed and the initial structural modulus (EI) may be obtained from the experiment and compared with the calculated value.

This procedure allows the estimation of the level of residual stresses of the as-built structure by the evaluation of the energy dissipated in each cycle of loading, which is given by:

$$E_d = \oint \vec{F} \cdot d\vec{z} \qquad (1)$$

F is the vertical load and *dz* the increment on the vertical displacement at the loading point. Figure 5 shows the load-global vertical displacement relationship obtained in the first three cycles of loading.

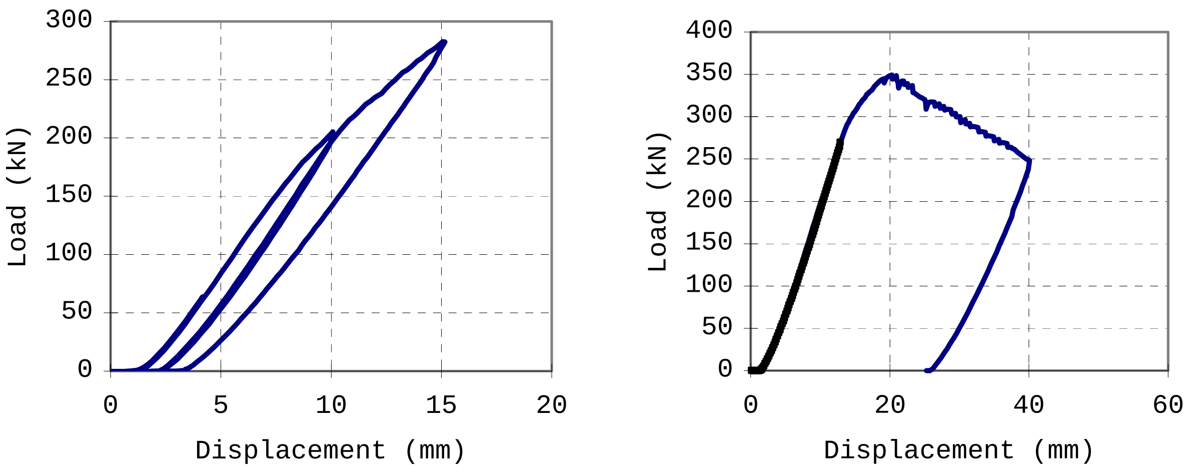

Figure 5 – Loading cycles until 60, 200 and 280 KN (left) and final cycle (right).

According to the usual model of residual stresses, the energy dissipates by plastic flow near the longitudinal stiffeners at the bottom, which is in compression. According to the same model it is not expected to have any relief of stresses at the top, which is in compression, at least for low load levels. The stress relief results in an increased residual deformation after each cycle.

The 4mm cycle only dissipated 6.2% of the total energy involved in the loading process and the residual deformation was 0.1mm. The 10 and 15mm cycles dissipate 22.8 and 23.3% of the input energy in each cycle, respectively. The residual deformations were approximated 1 and 2mm respectively. These results show that the idealized tensile block of the residual stresses (Gordo and Guedes Soares, 1993) was in the beginning of the test at a stress lower than the yield stress, otherwise the percentage of the dissipated energy should be above 20% on the first cycle. The Bauschinger effect is of little magnitude compared to the energy dissipated by plastic deformation near the welding.

The ultimate load was obtained at a nominal displacement of 20mm and a corresponding load of 350kN.

3.1 Moment curvature relationship

In order to obtain the moment curvature relationship it is necessary to transform the load to moment and to measure the curvature of the model. The bending moment is given by $M = Fl/2$ where l is the distance between the loading point and the support. The curvature was obtained from two independent gauges located at both sides of the loading points that allow getting the average curvature across the model. Due to symmetry it was expected that both gauges indicated the same curvature. However that was not the result and some transverse rotation was detected associated with the imposed curvature.

Figure 6 shows the relation measured in both gauges (R1 and R2). The gauge 1 indicated a higher curvature than gauge 2 until collapse (20mm displacement), but after this point the rotation was reversed. On the very deep collapse region the second gauge failed to work properly and an extrapolation was introduced based in the very strong correlation between gauge 1 and 2 before that point (R2c=1.98967xR1-0.00684), but it only affects the region of the unloading at the end of the experiment.

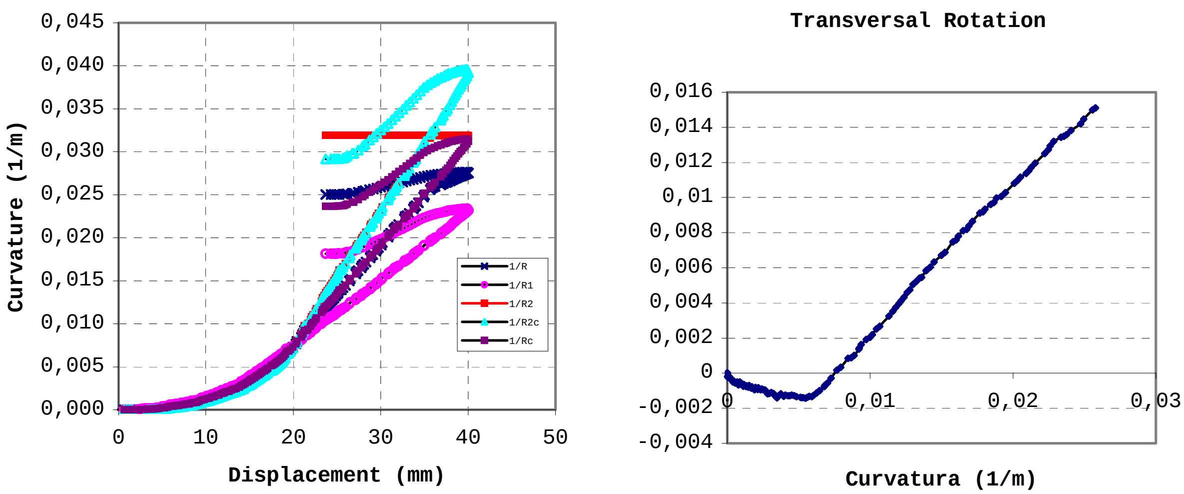

Figure 6 – Relationship between curvatures, displacement and transversal rotation

The moment curvature relation presented in figure 7 includes the extrapolation (Rc). This curve shows four typical regions. The first one until 160kNm is linear and of very high rigidity, EI=196MNm^2.

The second region is also nearly linear ranging from 160 to 290kNm, but it presents a lower rigidity than the first one. The reduction on the slope of the curve is mainly due to the reduction on the effectiveness of the panels under compression as a consequence of the development of out-of-plane deformations as load increases. Residual stresses on the panels under tension do not contribute to this reduction because they were eliminated in the previous cycles of loading. The average structural modulus in this region is 68.5MNm^2, which is approximately one third of the value obtained in the first region.

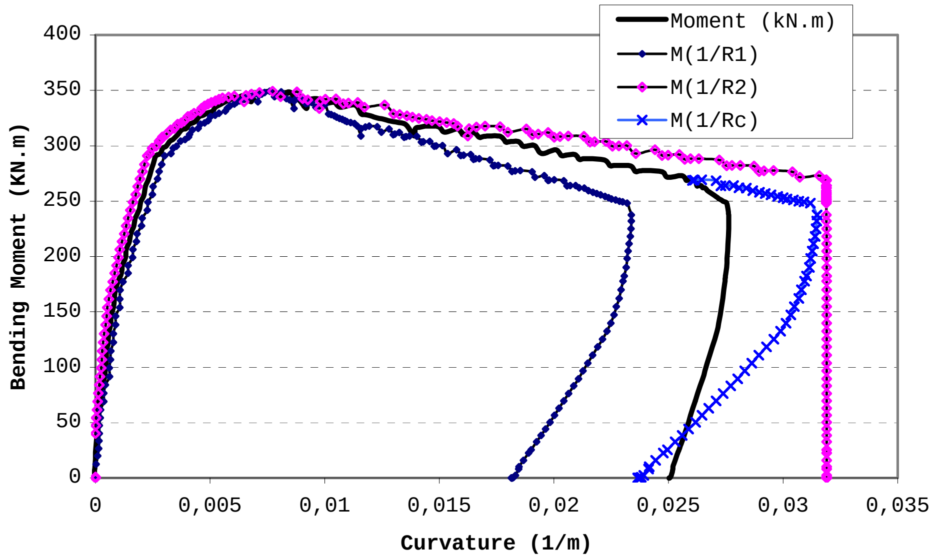

Figure 7 – Moment curvature relationship

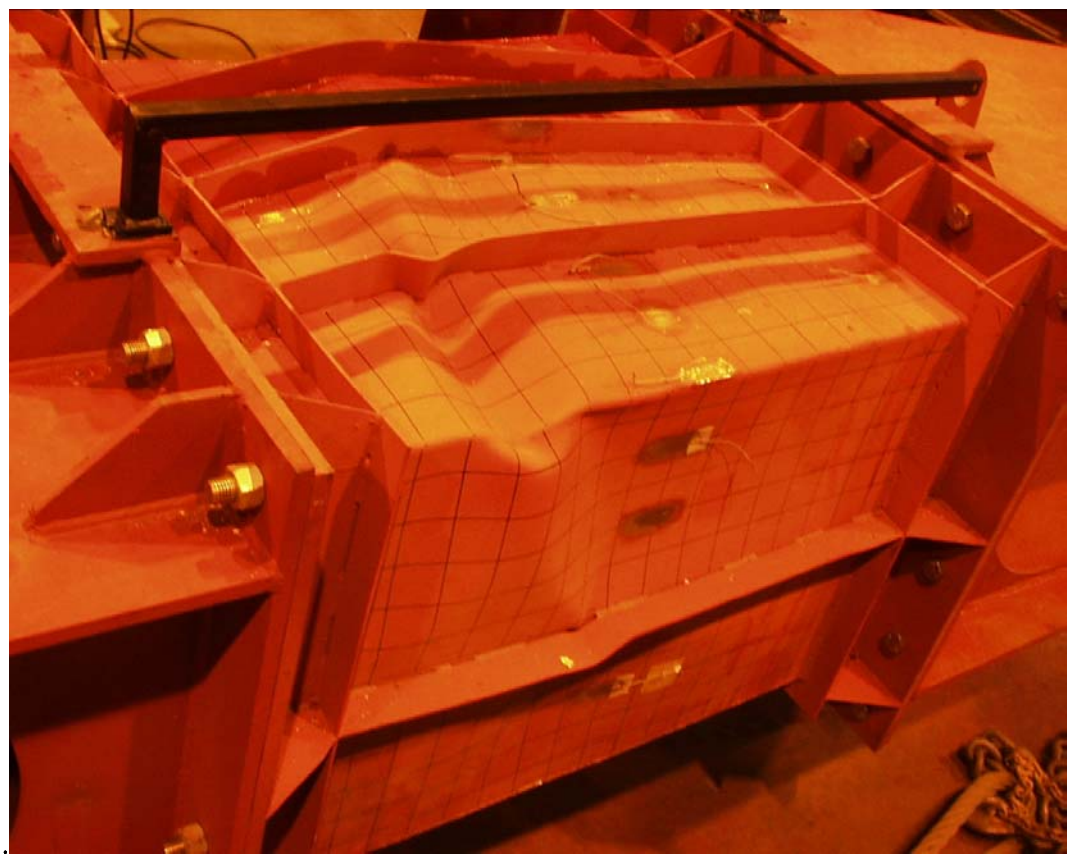

Figure 8 – Permanent deformation of the model after collapse. In black, at the top, there is the device to measure the curvature but without the gauge in the right extreme.

The third region goes until the ultimate bending moment of the structure, which has a value of 349.1 kNm at a curvature of 0.00767rad/m. The curve shows a non-linear behavior with decreasing rigidity, due to the plastic deformation of the residual stressed tensile strips and the loss of effectiveness on the panels under compression

At last, one has the shedding region where the moment supported by the structure depends linearly on the curvature, reducing progressively. This is the region associated with the development of very large permanent deformations, Figure 8. The discharge of the load shows two different regions: the first at higher load has high slope, but when the bending moment goes below 250kNm the slope reduces very much. The first corresponds to the elastic unloading of the very deformed panels and on the latter that panels are absorbing energy from unload of the rest of the structure which is still unloading in the elastic domain.

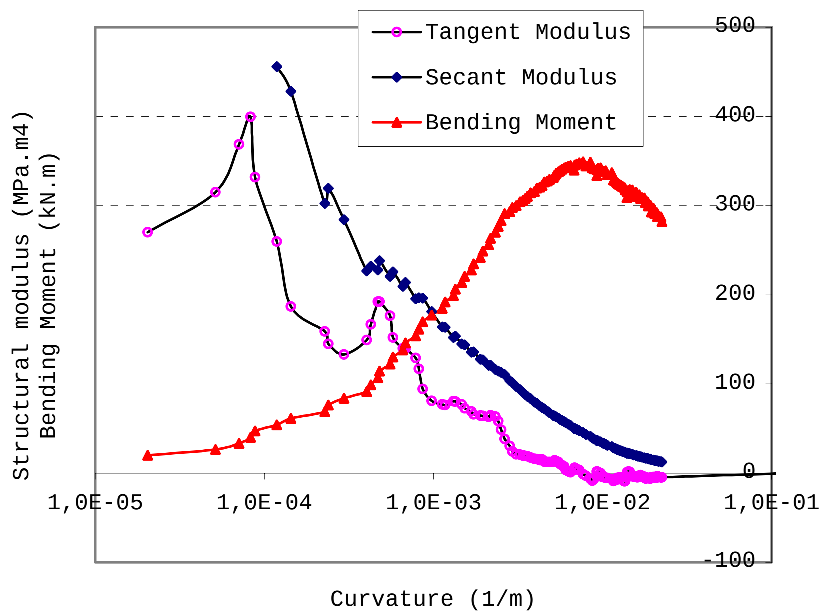

Figure 9 Tangent and secant modulus

3.2 *Structural modulus*

The linear theory estimates a structural modulus of 151MNm², assuming that the Young's modulus of the material is 210GPa, for a structure free of residual stresses and initial imperfections. For the real structure the tangent modulus is defined by $dM/d\phi = EI_e$, where M is the bending moment associated to the curvature ϕ and I_e is the effective inertial moment. The secant modulus is given by $M_s=M/\phi$, which is always positive and it is not so important as the first but one may refer to two particular values of secant modulus to obtain a quick approximation to the actual curve: the secant modulus at the first yield and at the collapse point. The results obtained from the experiment are plotted in Figure 9 in logarithmic scale of the curvature.

From the analysis of the graphic it may be identified the existence of several levels of the structural tangent modulus that may be related to the initial cycles of loading. At very low loading the modulus is very high and it seems to be related to the 4mm cycle. However one should not trust much on this initial measurement because it is possible to have some adjustment in the early stage that influences the measurement of the curvature gauges. The second plateau is in the range of the 10mm cycle and has values of the tangent modulus very close to the initial estimative from linear theory. The slightly decreasing plateau around 0.001rad/m has a minimum value of 63MNm^2 and seems to be connected with the 15mm cycle. In conclusion it seems that initial cycles generate some memory effect by stabilizing different geometric configurations due to the plasticity involve in each cycle by release of residual stresses.

3.3 Shift of the neutral axis

On an actual structure with residual stresses, the neutral axis is defined as the set of points where the strain is kept constant during loading. The position of the neutral axis may be estimated from the experimental data using the strain gauges located at the side shell of the box girder. These gauges were located at 140, 281, 410 and 508mm above the bottom plating and they allow the determination of the position of the neutral axis during the loading and to detect the loss of effectiveness during the elasto-plastic phase.

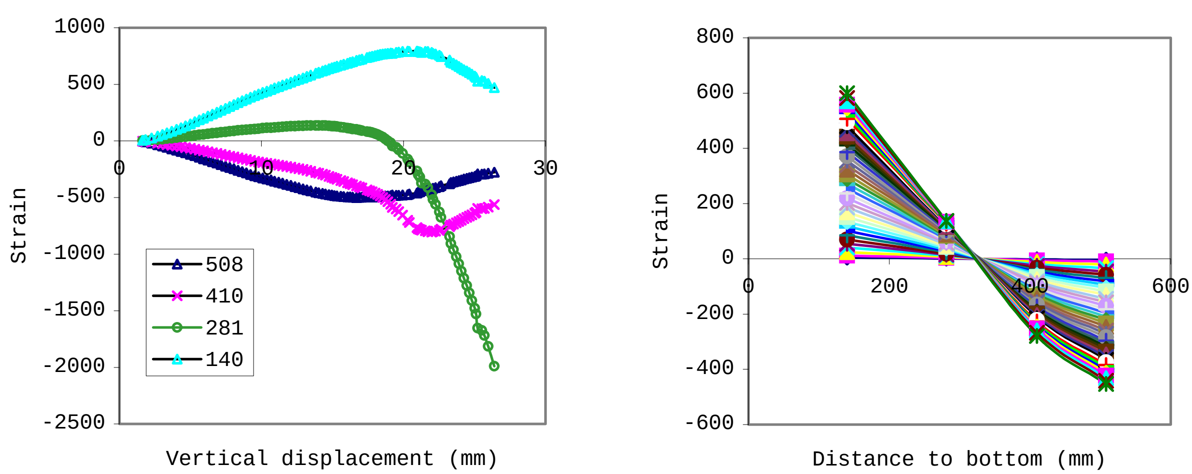

Figure 10 – Evolution of the strain at the side shell (until 14mm of the global displacement on the right)

Figure 10 presents the readings of those gauges. It may be identified a linear range until 15mm, which is the maximum loading point of the previous loading cycle, followed by a non linear region where initially the neutral axis drops its position. After 17mm the measurements are dominated by the out of plane deformations of the side shell that are induced by the deformations of the top panel in compression. It shall be noted that the strain is measured in micron and 1000 micron are approximately related to 200MPa. The strain gauge located at 281mm shows a very quick change after the collapse (20mm) because it is located on a plastic hinge line coming from the region at the top where the plate collapsed, Figure 11.

The gauge located at 510mm presents some loss of effectiveness even in the early stage of loading, which means that the distribution of strain becomes non linear in that region. It is possible to identify a small shift in the neutral axis towards the bottom due to that reduction of effectiveness in the top under compression.

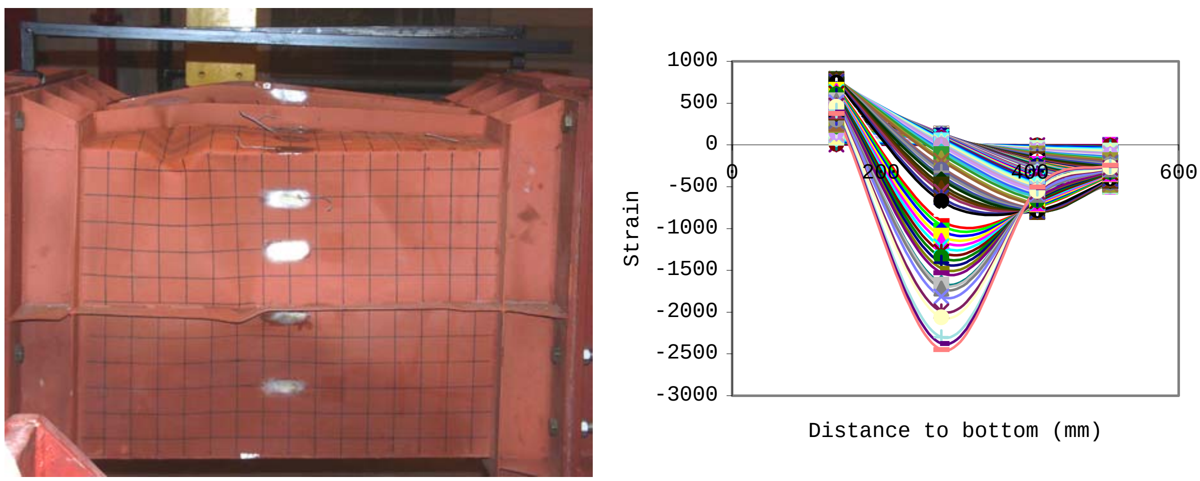

Figure 11 – Side view of permanent deformations of the specimen after collapse and evolution of the strains until very deep collapse.

The strain values at the plating surface are different from the average strain. Thus the readings include the membrane strain and the bending strain resulting from deformations of the box. For vertical displacements higher than 16mm the second becomes more important than the first. Thus the measurements on the gauge furthest away from the neutral axis (510mm) are lower than the readings on the gauges at 410 and 281mm.

The readings until 15mm may verify the position of the neutral axis while, from that point on, they are more associated with local deformations due to the buckling.

The strains are greater than the yield strain (885microns for this steel) at the central part of the side plating, reaching easily three times the yield strain in deep collapse.

4 Evaluation of residual stresses

The evaluation of the residual stresses in an indirect way is not very precise and requires the imposition of some hypotheses to simplify the problem. In this work two methods are presented and used for this purpose: the structural tangent modulus method and the total energy dissipation method.

The first one considers the variation of the tangent modulus at a point of a cycle corresponding to the maximum loading point in the previous cycle. The variation of the tangent modulus is the result of the variation on the effective inertia of the section due to the development of local plasticity at points where residual stresses are still high. There are, however, some direct effects that are not accounted for, like the modification of the geometric deformations due to the permanent elongation at tension of the residual stresses pattern.

The required data for this method are the experimental moment curvature relationship, the model of residual stresses due to welding and the material behavior, i.e. normally, the yield stress and Young's modulus assuming an elastic perfectly plastic material behavior.

It is assumed also that the variation of the structural tangent modulus at that point of loading is not affected by the non-linearity resulting from the loss of effectiveness in the panels under compression, but only from the plastic deformation of the tensile strips of the panels under tension. This assumption is sufficiently accurate for loads below the loading corresponding to the development of large deformations in the panels under compression, i.e., below the critical load.

4.1 Structural tangent modulus method

The cross section of the box is considered to have two regions. One includes all areas affected by the weld heating where initially the residual stresses are in tension at levels close to the yield stress and belonging to the panels under tension during the loading path. A_p designates the total area. A_e designates the remanescent 'effective' area of the box girder.

The structural tangent modulus in the elastic domain is described by:

$$EI_e = E\int_{Ae} z^2 dA_e + E\int_{Ap} z^2 dA_p \tag{2}$$

where z is the vertical distance of the center of the element of area to the neutral axis. The second term vanishes in the elasto-plastic domain due to plasticity occurring on the A_p region and the neutral axis changes its position from a distance δ, having for this situation:

$$EI_p = E\int_{Ae} (z + \delta)^2 dA_e \tag{3}$$

If the area A_p is small in comparison with the total area, then δ is of second order and the structural modulus may be estimated in an approximate way by:

$$EI_p = E\int_{Ae} z^2 dA_e \tag{4}$$

Thus the variation of the structural tangent modulus is approximately given by:

$$\Delta EI = EI_e - EI_p = \int_{Ap} z^2 dA_p$$

$$or \quad (5)$$

$$\Delta EI = Ez_p^{\ 2} A_p$$

assuming that A_p is located at the bottom of the model at a distance z_p from the neutral axis. Finally the area plastically affected may be expressed as:

$$A_p = \frac{\Delta EI}{Ez_p^{\ 2}} \quad (6)$$

From symmetry z_p may be considered to be as the model half height or it may be directly evaluated from the experimental values read in the strain gauges located on the side plating.

The method was applied using three points of the moment curvature curve close to the vertical displacement of 15mm, which is the last point of the loading at the previous cycles. Considering the data collected, P1=(0,00196rad/m; 249,0KN.m), P2=(0,002634rad/m; 290,8KN.m) and P3=(0,00343rad/m; 315.8KN.m), the variation of the structural tangent modulus was calculated around the point P2 and a value of 30.8MN.m^2 was obtained. It results from a structural tangent modulus before the point P2 of 62,2MN.m^2 and after of 31,4MN.m^2.

The area A_p is 962mm^2, according to the above equation considering a value of 200GPa for the Young's modulus and evaluating the neutral axis from the experimental data, that is 400mm above the panel under tension. This area includes the plastic deformation on the bar stiffeners. In order to estimate the residual stresses it was considered that there is a percentual equivalence between the tension strip areas of stiffeners and of the plate elements. The calculated compressive residual stress was 33% of the yield stress.

4.2 Dissipated energy method

The second indirect way of evaluating the level of residual stresses is based on the dissipated energy on each cycle of loading. It is considered that the material has an elastic perfectly plastic behavior and the neutral axis does not move during the loading path.

The dissipation of energy occurs on tension strips of the residual stress pattern of the bottom and it may be evaluated by equation (1). The results are summarized in table 2.

Table 2 - Dissipated energy per cycle of loading. Energy is expressed in J.

Displacement (mm)	Total Energy	Dissipated Energy	Ed/Et (%)	Total Energy per Cycle	Dissip. En. per Cycle	EdC/EtC (%)
4,18	82,4	5,1	6,2	82,4	5,1	6,2
10,08	898,8	209,3	23,3	893,7	204,2	22,8
15,16	2167,1	661,6	30,5	1962,9	457,4	23,3

These values may be compared with the theoretical value calculated from the hypotheses mentioned before:

$$E_d = \sigma_o A_p \Delta l_p \tag{7}$$

where l_p is the frame span for continuous welding or the total length of welding for discontinuous welding. This equation may be rearranged according to the geometry of the test models:

$$E_d = \sigma_o A_p l_p z_p \phi \tag{8}$$

The total area of the tension strips at the bottom is:

$$A_p = \frac{E_d}{\sigma_o l_p z_p \phi} \tag{9}$$

There is information about three cycles of loading that can be used on this method: 4, 10 e 15 millimeters of maximum vertical displacement. Using an average value for the yield stress obtained in the tensile tests, corrected proportionally by the higher yield stress of the 4mm bar stiffeners, one gets the value of 201MPa, thus the area A_p is 2283 and 2156mm^2 respectively for 10 and 15mm displacement cycle. These areas are much greater than the value obtained in the previous method because there are very heavily welded regions on the extremes of the model, which generates a large dissipation of energy during loading.

Taking into account the length of the transverse welds at the frames and extreme connections the calculated values of A_p reduce to 1087 and 1027mm^2 respectively at 10 and 15mm cycle. It gives a 10% difference between the two indirect methods thus one may consider that the compressive residual stresses are about 1/3 of the yield stress.

5 Effectiveness of the panel under tension

The panels under tension belonging to a structure subject to bending are normally considered to behave according to the linear theory of beams. If there is bending and shear acting together, one has shear lag effects that correspond to a redistribution of stress but if the loading generates pure bending then the distribution of stresses and strains on a panel located at constant distance from the neutral axis is considered to be constant and no lack of effectiveness is considered by the theory because the global geometry of the structure is considered to remain unchangeable. In the present case, test of a box girder under pure bending, some loss of effectiveness was detected that seems to be related to the lack of support in the middle of the panel under tension.

On the regions where there exists a connection with vertical components the curvature is equal to the global curvature but, in the absence of the vertical supports as it is at the middle, the local curvature becomes lower than the global curvature because the plate can find compatibility with a reduced deformation corresponding to lower curvature and lower strains. In the present case there are three main reasons for the reduction of the effectiveness at the middle of the panel:

1. Reduction of the initial imperfections at the middle of the panel due to tension of the plate. The contribution is not very important and reduces with the increase of the loading.
2. Reduction of the curvature at central part of the panel due to lack of vertical support. The reduction decreases with the increase in the number of stiffeners.
3. Plasticity on the tension strips of the residual stresses pattern, which conducts to the development of residual strains after a loading cycle and a decrease of the imperfections after unloading.

A set of strain gauges were installed on the bottom panel of the model M3-200 transversely aligned in order to allow tracking the evolution of the strain distribution during the loading cycles.

5.1 Initial cycles

Figure 12 shows the measurements obtained from the strain gauges for the three initial cycles of loading, i.e., 4, 10 and 15mm of vertical displacement.

In the first graphic, the transversal distribution of strain presents a magnification of the strain variability with the loading increase. One may note a global depression on the central part that grows when the loading increases and some local variability mainly associated with the presence of stiffeners. For this low loading it does not exist a direct relation between strain and deformation of the plating because the vanishing of the initial imperfections dominates the results. They depend very much on the location of the strain gauges, which are on one side of the plating, and if one of the gauges is initially located in a depression the local strain is above the average and vice-versa for a crest.

In this first cycle, the unloading did not generate residual strains, which means that the structure did not suffer great plastic deformations due to residual stresses. This is confirmed by the low value of the dissipated energy already mentioned in Table 2.

In the 10mm cycle, the strain distribution pattern is similar to the 4mm cycle one but having a much more increased inefficiency at the middle of the panel. The highest values in strain are located at the extremes of the panel at the connections with the vertical components, achieving 564 and 677 microns and below the yield strain of the material, which is approximately 900microns. But these values represent strain variation in relation to the initial strain state, thus it is possible to have already some plasticity in certain locations where the true strain is higher than the yield strain. It certainly happens in the tension strips of the residual stresses and it is confirmed indirectly by the residual values of strain after the total unloading. The average value of the residual strain is about 50 micron with maximum at the extremes of the panel reaching 142 and 66 micron. The maximum value of the residual strain was measured at the extreme of the panel where a corner welding is located for closing the box and thus it caused the residual stress relief.

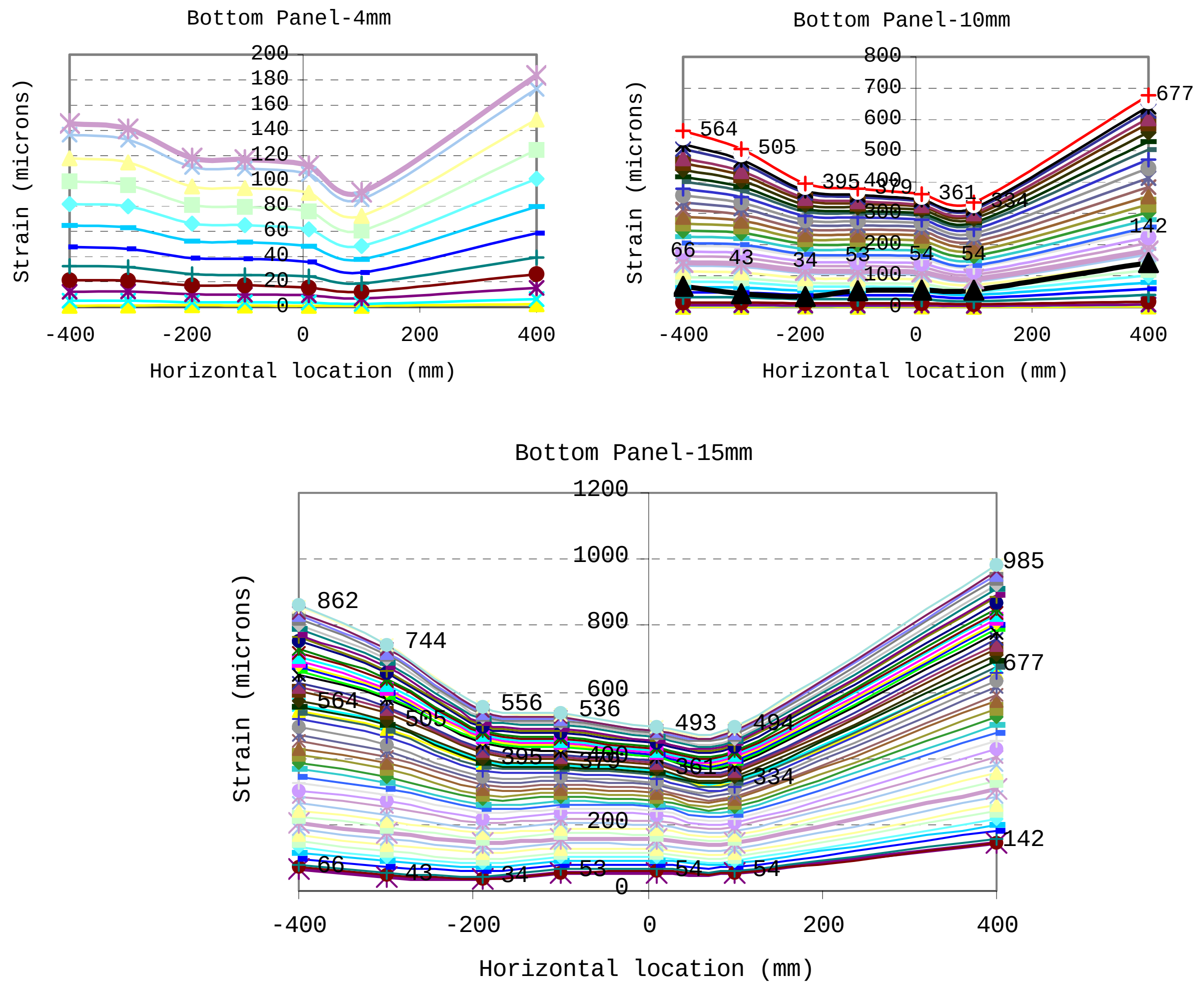

Figure 12 – Transverse distribution of strains at initial cycles

The last graphic of the same figure relates to the 15mm cycle and shows that the loading until 10mm is in elastic regime due to the similarity between the strain distribution of the previous cycle maximum and the closest curves of the 15mm cycle. The loss of effectiveness becomes more important after 10mm loading and the pattern becomes typically sinusoidal.

The average residual strain after the 10mm cycle allows the estimation of an increase of the length of the bottom panel of about 6% due to residual stress relief. This elongation due to stress relief leads to a redistribution of residual stresses in the whole box and a residual curvature. Globally the redistribution of stresses in the unloaded structure creates a compressive state of stresses on the bottom panel, followed by a region under tension on the side plating that tends toward a slightly compressive stress on the top panel.

5.2 Final cycle of loading

In the final loading cycle all transducers were reinitiated thus the presented measurements were subtracted from the residual values of the 15mm loading cycle and unloading. In order to obtain the absolute values relatively to the initial state the residual values should be added.

5.2.1 Strain gauges on the plating

Figure 13 presents the measurements obtained from the strain gauges located on the outer surface of the bottom panel. The position of each gauge is indicated in the legend and means the distance to the plane of symmetry.

The first conclusion that one may draw is that symmetric gauges indicate different behavior and the difference is more marked in the comparison between the gauges located in the extremes of the panel, respectively at -400 and 400mm. They have the same behavior until the yield strain is achieved, which happens at a vertical displacement of 15mm. From that point on, the strain read at the gauge located at 400mm (gauge T11) continues to be linearly dependent of the vertical displacement until the displacement of 22mm (strain of 1230 micron) reaching the maximum strain at 29mm with a value 1366 micron, which is the maximum point for all gauges readings. The different behavior between extremes is a result of different levels of residual stresses and, maybe, different material behavior. In one of the sides there is a welding to close the box and on the other side the corner was manufactured by bending the plate. Thus in one side there is no residual stresses while in the other they exist.

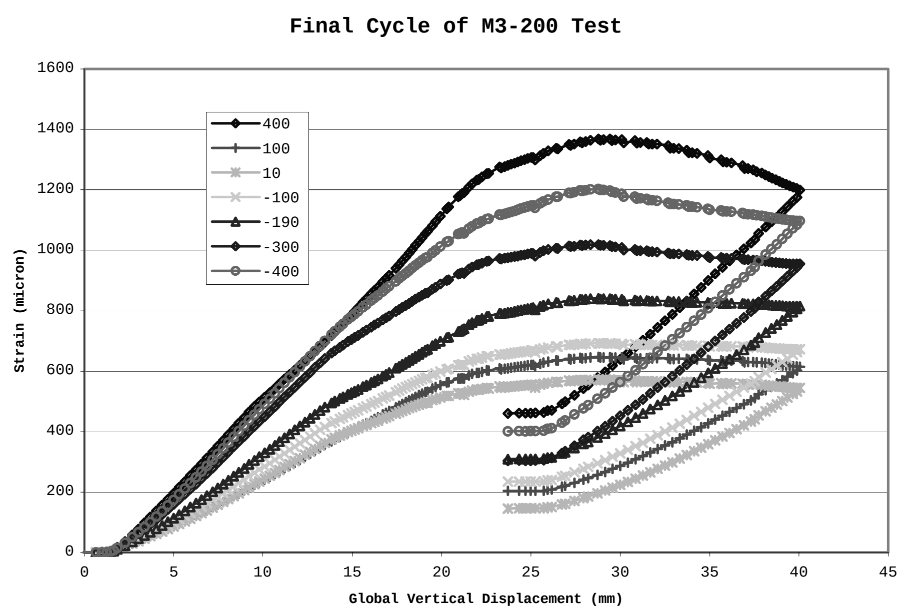

Figure 13 – Strain at the bottom panel during final cycle.

The ultimate carrying capacity is achieved at an absolute vertical displacement close to 21mm and in this phase the neutral axis shifts its position quickly in the direction of the bottom due to the decrease of effectiveness of the top panel in compression. Indirectly it affects the relation between the bottom strain and the curvature because they increase more slowly. This may be observed in the change of the slope of the curves in the same figure when the vertical displacement is between 21mm and 29mm. From this point, the increase in the rate at which the neutral axis approaches the bottom and the reduction in the supported bending moment (already shedding the loading) originate the stationary or even the decrease of stresses and strains in the bottom panel.

The two symmetric gauges located at the middle of the plates, 100 and –100mm, behave similarly during the test and they measured a residual strain after unloading of about 200 micron despite the yield strain not being reached during the loading. The maximum strain at those locations was 700 micron.

The strain distribution along the breadth of the panel is presented in Figure 14 for the final cycle, for which the applied displacement had double the displacement corresponding to the collapse. It is evident the existence of two different regions in the plating: in the extremes the strains are very high, which means that it is very effective due to the presence of vertical support, and in the middle of the panel where the strain reduces to half of the maximum values. The local variations tend to disappear when entering in the post collapse domain and the distribution tends to be linear between the extremes and the middle.

The presence of the longitudinal stiffeners is not very marked in the loading phase, but the final state after unloading shows that near the stiffener (positioned at –200mm) there are an increase of the residual strain compared to the global tendency.

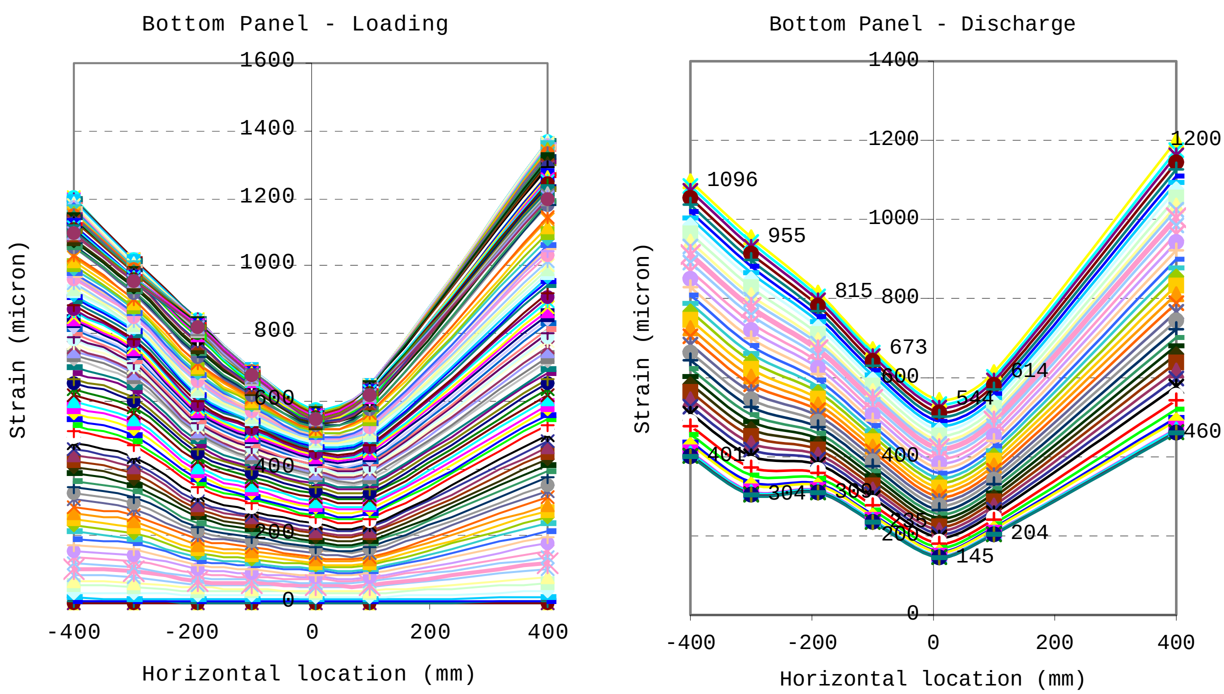

Figure 14 – Strain distribution at the bottom panel in the final loading cycle.

The residual strain values are very high varying between 145 micron in the middle to 460 micron in one of the extremes, both in tension. This last value is half of the yield strain but real elastic strain should be approximately 140 micron without allowance for hardening of the material during plastic straining. This value is consistent with the measurements at the middle of the panel where no plastic deformations had occurred. This residual elastic tension strain needs to be equilibrated by some compression of the structure in the vicinity since no external force or moment is applied. Those regions are the side shell and eventually the bottom stiffeners.

In conclusion the state of strain and stress of a panel in tension due to applied pure bending moment is far from being uniform. The plating is more effective in the regions where there are vertical components like webs or stiffeners.

5.2.2 Stress redistribution

The design of the box girder considers a space of 100mm on each extreme of the specimen in order to obtain a good transition from the supports to the test region.

In order to verify the quality of the connection and its ability to transmit and redistribute the loads, a set of strain gauges were mounted close to the transverse frames referred as T00, T01, T04, T05 e T08.

The analysis of the readings of the strain gauges, Figure 15, indicates a big difference of the strain at gauge T00 located close to the side of the box in comparison with the others. This gauge indicates strains that go until 3200 micron at the point of the collapse of the box girder. This value is almost four times the yield stress and thus it corresponds to large plastic deformation near the sides pointing to heavy distribution of loads at those points in comparison with the middle of the plating near the frames.

The others present normal values when compared with the readings at the gauges located in the middle of the plating, far away from the frames. However they seem to be lightly loaded until the last cycle's displacement (15mm) is achieved. This is more marked for the gauges T04 and T08 that are located near the longitudinal stiffeners and confirms some memory of the structure in relation to the previous cycles of loading. The gauge T05, located in the center but far away from the stiffeners shows some loading absorption in the initial phase but with a low slope.

Thus it seems that the presence of the longitudinal stiffeners affects the stress state of the plating and the behavior shall be analyzed considering both acting together.

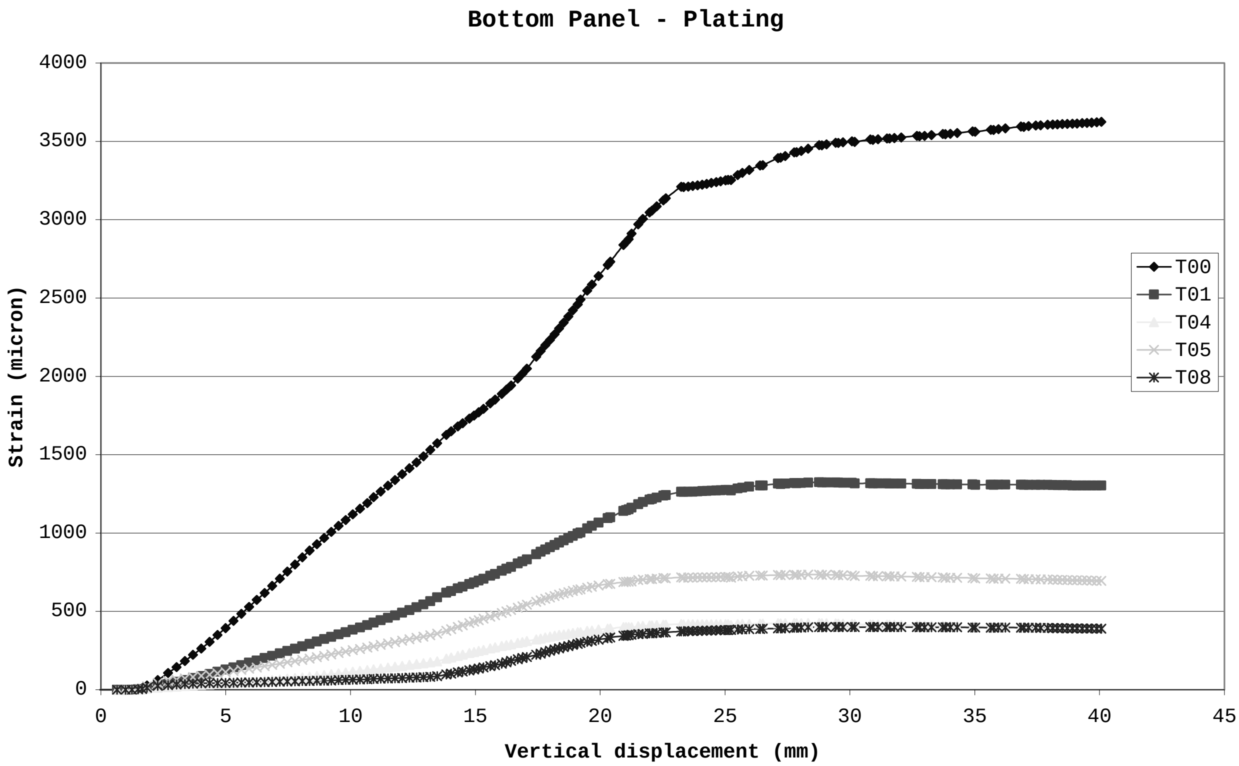

Figure 15 – Readings at the strain gauges located near the transverse frames of the bottom panel

5.2.3 Longitudinal stiffeners behavior

Three strain gauges were installed on the longitudinal stiffeners, in a lateral position near the top of them. Two of them, TR00 and TR02, were located at the middle span of the stiffeners and on the vertical of the plate gauges T06 and T09, respectively. The other gauge was located close to the transverse frame over the gauge T08. The arrangement allows to analyze the different loading stage of the different stiffeners at the middle span, the variation in the longitudinal direction and to compare the load supported by the stiffener and the plating.

The stiffened plate is a three dimensional structure supported by the frames. Close to the frames the level of rotational clamping due to the stiffener is much more efficient than the clamping due to the plating, thus the stress level on the stiffener should be higher than that on the plating. In fact, Figure 16 shows a very big difference between the strain level on the stiffener (TR01) and on the plating (T08) at the same location. The former is heavily loaded with a linear performance until 14mm vertical displacement while the latter is comparatively almost unloaded.

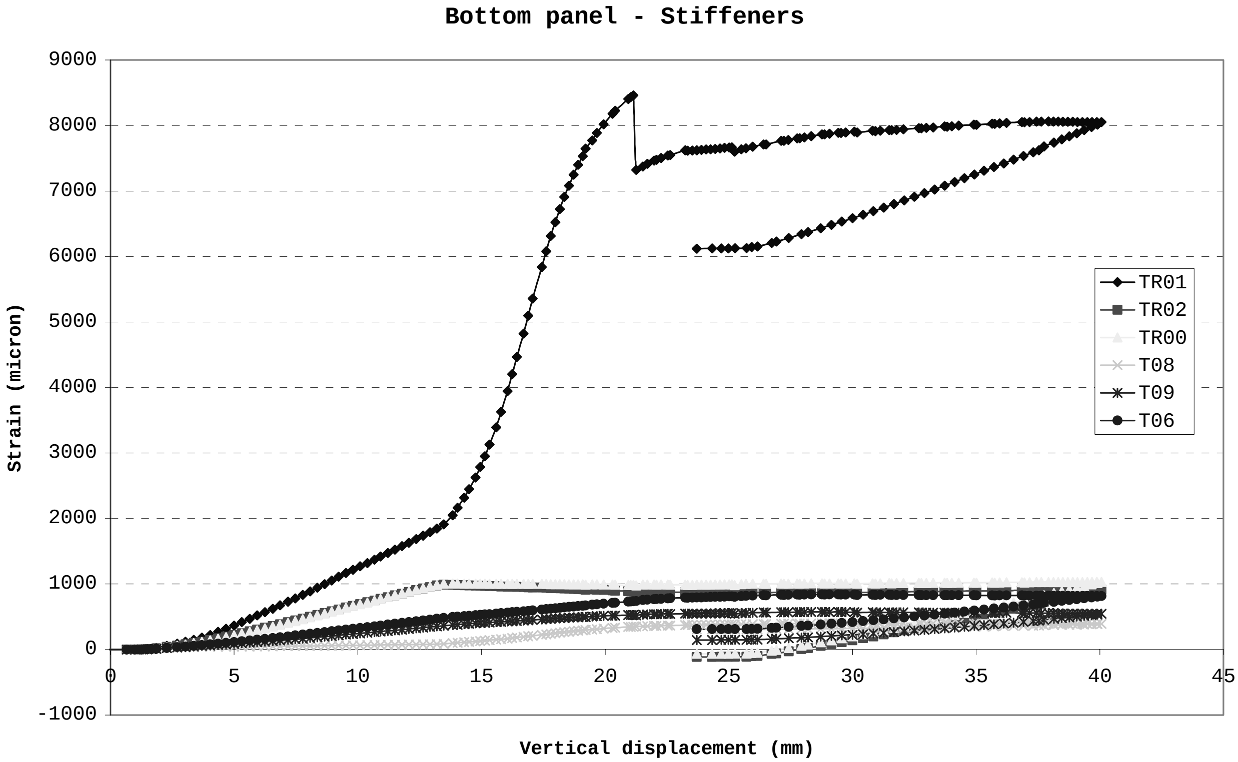

Figure 16 – Axial strain at the longitudinal stiffeners (TR) and nearby plating (T)

Once the maximum limit of the previous cycle is overridden, the stiffener strain (TR01) near the frame rises to very high values in the plastic range, reaching almost ten times the yield strain. At collapse there is a sudden decrease in the strain at levels of the yield strain, which means that the stiffener was at that time without carrying any load. This sudden unloading may be originated by a crack in the welding or by the development of large deformations that come from the top to the bottom panel.

Figure 17 presents only the readings at the middle span of two stiffeners and associated plate. In both stiffeners the strain grows linearly until the yield strain, which is achieved at the maximum of the previous loading cycle and after that point they stay almost unchangeable until the maximum imposed displacement. The rate of unloading is typically of the same magnitude of the loading rate. This means that after the 14mm displacement the stress level in the stiffeners was almost the same during the loading path and even for the central stiffener (TR02) some decrease of strain (stress) was noted until the collapse of the box. The strain rate in the stiffeners is much higher than in the adjacent plating, which must result from the different rigidity under bending.

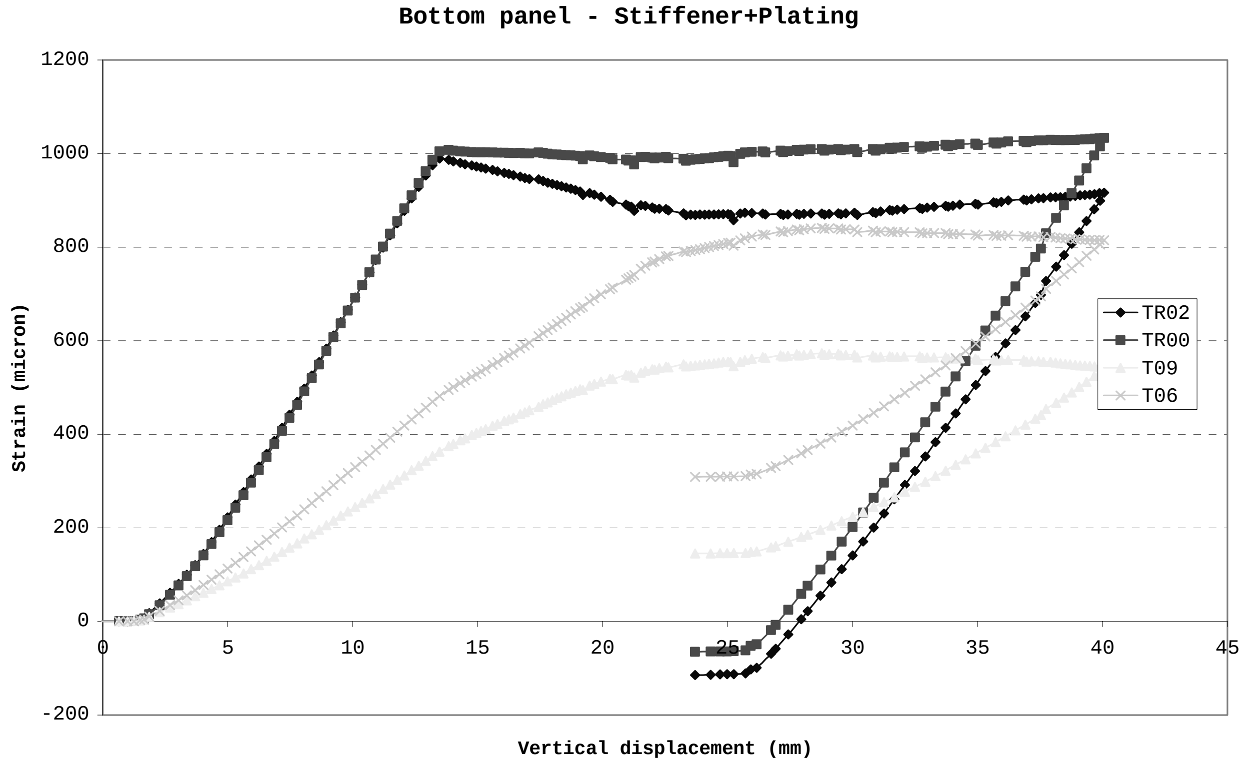

Figure 17 – Strain at middle span on the stiffener and plating

5.3 Top panel under compression

The top panel, which is under compression when the box is bend, had 23 strain gauges installed, five of them on the stiffeners and the rest on the out surface of the plating. Two sets of gauges were installed in transversal alignment in order to get the strain distribution at the middle and next to the frame. Due to the expected nature of the buckling mode, a third set was installed 100mm away from the central set, in an attempt to obtain a general information about the strain distribution in the case of having a localized collapse over one of the previous principal set of gauges.

5.3.1 Set of strain gauges near the frame

The reduced number of gauges (5) installed near the frame just allows a general overview about the evolution of strains during the test. The local distribution is better represented in the left side due to the presence of a supplementary gauge near the stiffener (position -200). The three gauges located around that position (-300, -200 and -100) give an idea about the distribution of strains in a typical stiffened plate element, see Figure 18.

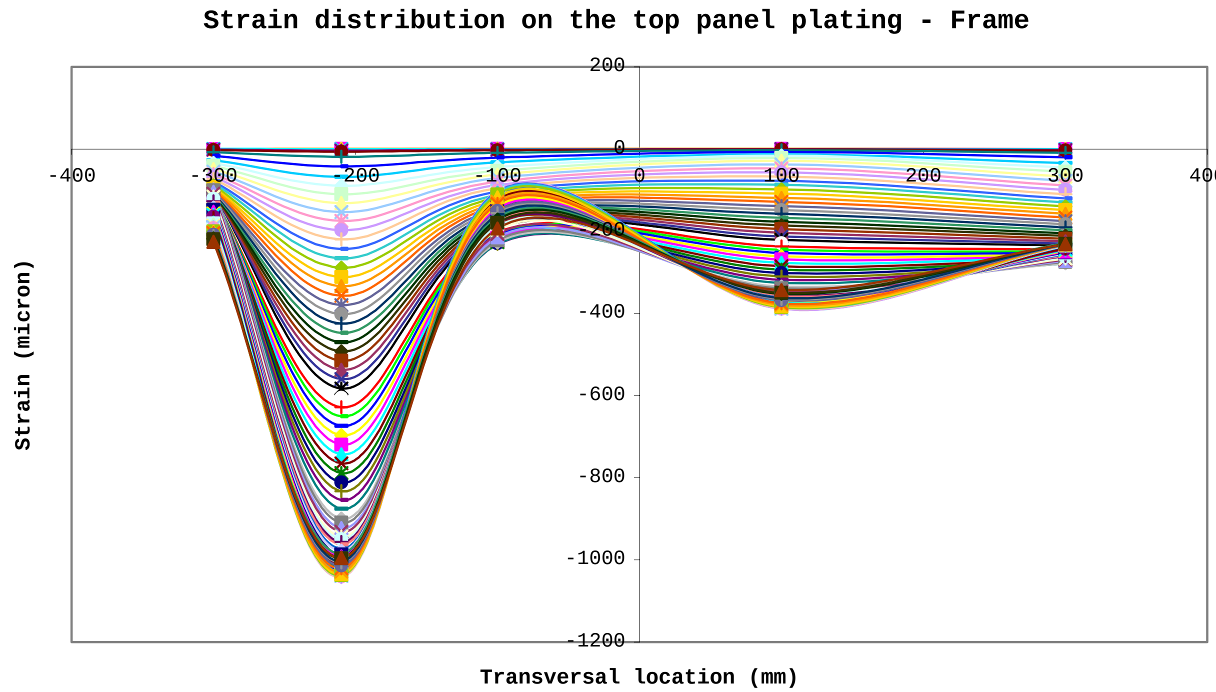

Figure 18 – Strain distribution on the plating of the top panel measured 50mm apart from the frame until the ultimate bending moment is reached.

There is a lack of effectiveness in the initial stage of loading in the middle of the plate elements (positions -300 and -100mm) comparatively to the plate near the stiffener (position -210mm). When the collapse is achieved only one of the five reading points is apparently under plastic deformation, which is in fact the only strain gauge located near the stiffener. Thus it may mean that near the other stiffeners (positions 0 and 200mm) the same behavior may occur. One may also note the low level of strain at the middle of the plate elements, but the those values must be updated with the residual strains due to welding, which were not shake down in the previous cycles of loading on this panel.

5.3.2 Central set of strain gauges

In the middle span of panel it was installed a set of nine strain gauges located alternately at the middle of the plate and at the plate near the stiffeners. Figure 19 presents the readings on those gauges as a function of the imposed vertical displacement.

One may identify four main phases on the evolution of the strains in the plating: the first phase goes until 14 mm of global vertical displacement and the dependency of the strain relatively to the displacement is almost linear, but two gauges on the center of the plate elements (C02 and C12) present positive readings growing with the loading. This is due to the existence of residual deflections resulting from the initial cycles of loading with local concavity towards the inner part of the box and sufficiently high amplitude that generates positive strain due to bending increasing the local curvature which is able to eliminate the negative strains resulting from the compression of the panel. At the final of this phase some of the strains are very close to the yield strain of the material.

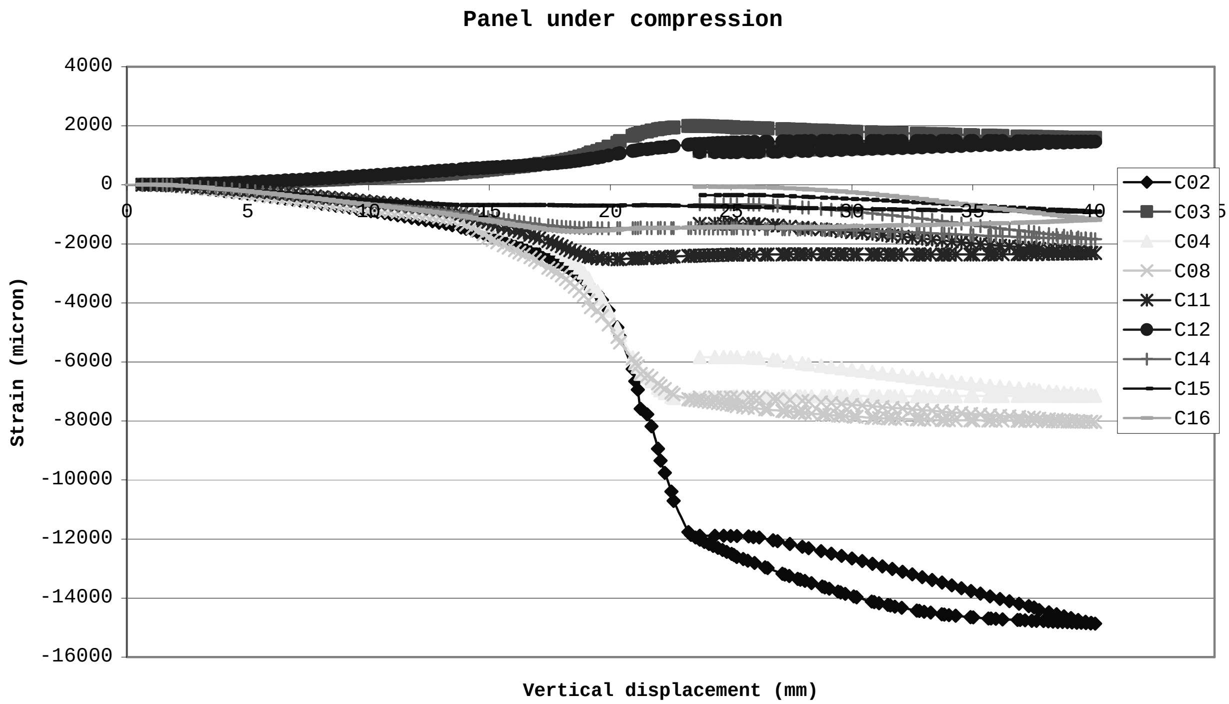

Figure 19 – Measurements of nine gauges located on the top panel at a middle span, until the maximum external displacement applied (40mm), followed by the withdrawal of the loading.

The second phase ranges approximately from 14 to 20mm. The rate of the increase of the strains with the displacement grows very much, which means that the out of plane deformations are growing in the same way.

The third phase is very short corresponding to the development of the global collapse of the top panel associated with strains that exceed largely the yield strain, more than fifteen times in the case of gauge C16.

The last stage corresponds to the post collapse regime, where the strains in this panel are stabilized or even some of the gauges present a decrease in the strains (C11, C16, C15 and C14). The strain gauges C02 and C08 show some increase in strain due to the fact that they are located where the collapse continues under development, i.e., in regions close to the plastic hinges.

Figure 20 shows the evolution of the strain distribution across the top panel until the ultimate bending moment is reached. The plastic hinges associated with the very large deformations observed are located on the left side of the figure.

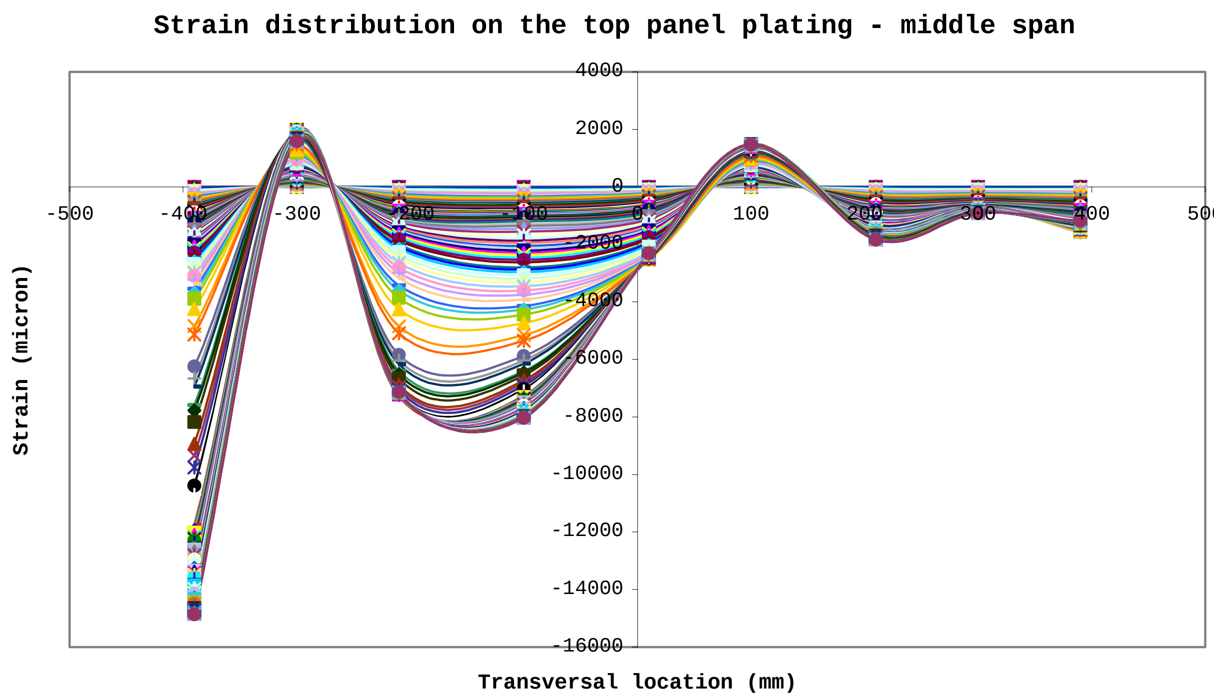

Figure 20 – Strain distribution on the plating of the top panel measured at middle span until the ultimate bending moment is reached.

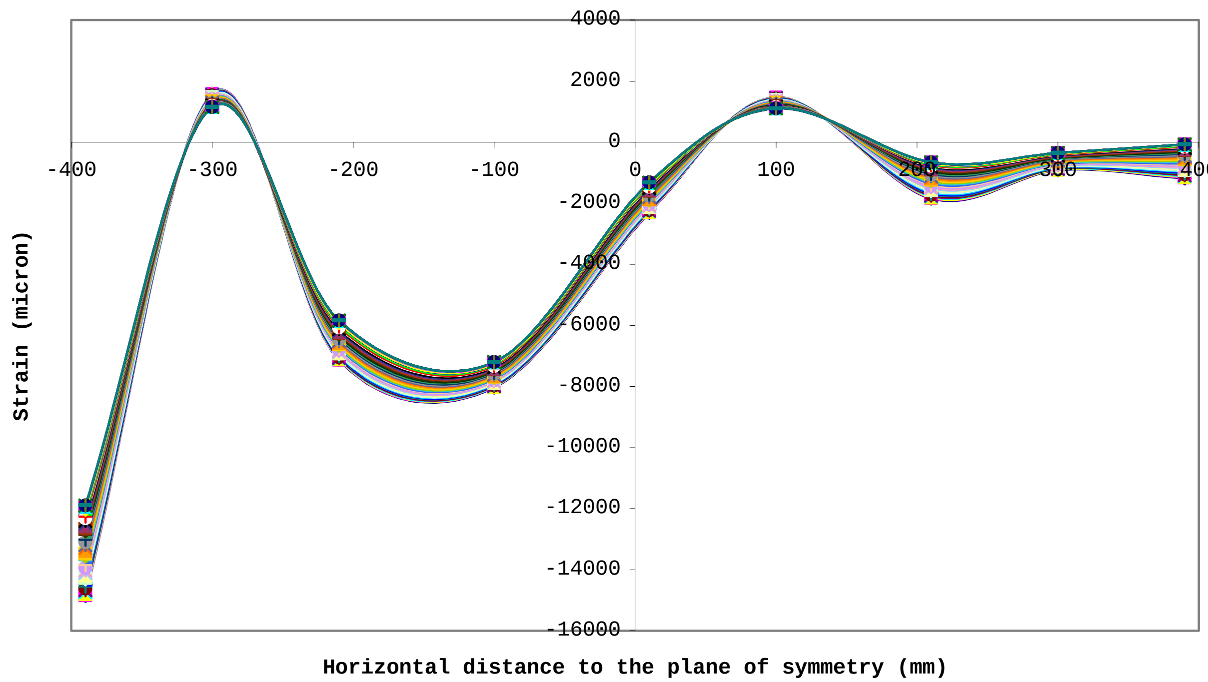

Figure 21 – Strain distribution during unload and residual values

The residual strains after unloading are very high and are almost equal to the maxima observed during the experiment, Figure 21. This means that there was not much change on the deformed geometry after the total unloading and the reduction on the strain is only due to the release of the accumulated elastic energy.

5.3.3 Stiffeners

Four strain gauges were installed at the middle span of the stiffeners. They allow measurements of the strain in both sides of the central stiffener through the gauges CR03 and CR04, which give the ability to calculate the average strain and the strain associated with an eventual bending of the stiffener. The other two (CR00 and CR05) were located on the same side of the other two stiffeners as the CR03.

According to the theory, most probably, the gauges CR00, CR04 and CR05 will give the same readings because it is expected to have symmetry in consecutive stiffeners. In fact that may be observed in Figure 22 until the collapse phase when some plasticity has already occurred.

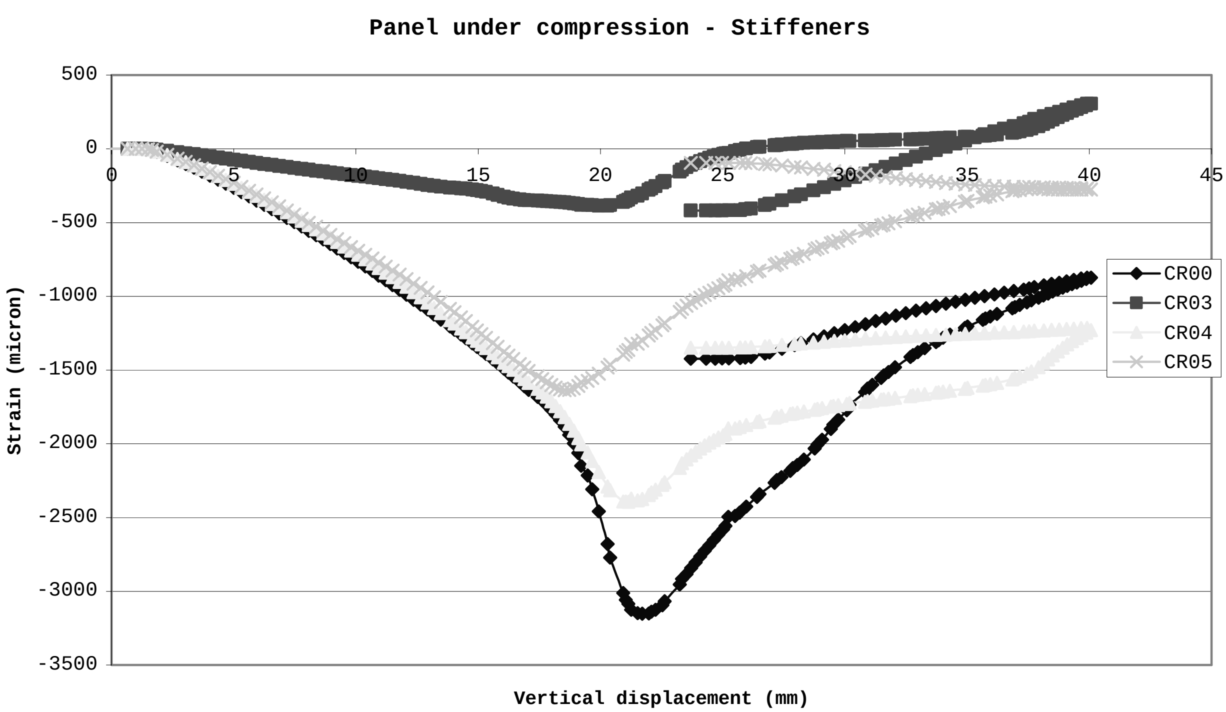

Figure 22 – Strain gauges readings at the middle span of the stiffeners of the top panel.

The right stiffener (CR05) lost efficiency at an early stage of loading (18mm of applied displacement), which means that there has been a local failure.

It is interesting to note that some compression occurs during the unloading of the two other stiffeners that are associated with the gauges CR00, CR04 and CR03. This local compression occurring during unloading results from the deformed geometry of the structure after buckling, in which the top panel deformed to the outside. Thus in the post collapse region the increase in the deformations tends to generate tensile strains on the top of the stiffeners that have to be summed to the compressive strain due to bending resulting in a reduction of the total strain as the global curvature increases. For the gauge CR05 the process of unloading conducts to normal behavior with a reduction of strain, but the local permanent deformations were different than those on the rest of the top panel.

6 Conclusions

The results of an experiment of a box girder subjected to pure bending moment are presented. This experiment was chosen to be representative of the conditions that can occur near the midship region of conventional ships or FPSO's. The moment curvature relationship was established until the region of large permanent deformations, allowing defining precisely the behavior in pre and pos collapse ranges. Two methods were presented to evaluate indirectly the level of residual stresses from the experimental data and good agreement between them was obtained. Large residual stresses relief is obtained in the panels under tension if initial loading cycles are applied. These initial cycles seem to generate some loading memory on the structure, which influences the moment curvature relationship.

The transverse distribution of strain at the middle of the box girder shows a loss of effectiveness of the stiffened panels under tension in regions far away from the main vertical plating (webs) and at high applied moment. Strains in the middle of panel may be half of those found at the corners. The strain pattern remains after unloading.

In the panels under compression the strain distribution is less affected by the initial loading cycles but large plastic strain develops during the collapse phase. The geometry of the buckled structure compares well with the distribution of the residual plastic strain after collapse and unloading.

Ackowledgements

This work has been funded by Fundação para a Ciência e Tecnologia through its Plurianual funding to the Unit of Marine Technology and Engineering.

7 Reference List

Adamchak, J. C. An approximate method for estimating the collapse of a ship's hull in preliminary design. *Proceedings Ship Structures Symposium '84*. **1984**; 37-61.

Billingsley, D. W.. "Hull girder response to extreme bending moments". *Proceedings 5th*

STAR Symposium: SNAME; **1980**: 51-63.

Caldwell, J. B. Ultimate longitudinal strength. *Transactions of RINA*. **1965**; 107:411-430 .

Dow, R. Testing and analysis of a 1/3-scale welded steel frigate model. *Advances in Marine Structures 2*. C.S. Smith and R.S. Dow eds. Elsevier Applied Science; **1991**; pp. 749-773.

Dowling, P. J.; Chatterjee, S.; Frieze, P., and Moolani, F. M. Experimental and predicted collapse behaviour of rectangular steel box girders. *Proceedings International Conference on Steel Box Girder Bridges*. London; **1973**.

Faulkner, D. contribution to the discussion of "Ultimate longitudinal strength" by J. Caldwell . *Transactions of RINA*. **1965**; 107.

Gordo, J. M. and Guedes Soares, C. "Approximate load shortening curves for stiffened plates under uniaxial compression". *Integrity of Offshore Structures – 5*, D. Faulkner, M. J. Cowling A. Incecik and P. K. Das.; (Eds) Glasgow. Warley, U.K.: EMAS; **1993**: 189-211.

Gordo, J. M. and Guedes Soares, C. Approximate method to evaluate the hull girder collapse strength. *Marine Structures*. **1996**; 9(1):449-470.

Gordo, J. M., Guedes Soares, C. and Faulkner, D. Approximate assessment of the ultimate longitudinal strength of the hull girder. *Journal of Ship Research*. **1996**; 40(1):60-69.

Guedes Soares, C., Dogliani, M., Ostergaard, C., Parmentier, G. and Pedersen, P. T. Reliability Based Ship Structural Design. *Transactions of the Society of Naval Architects and Marine Engineers*. **1996**; (104):357-389.

Nishihara, S. Ultimate longitudinal strength of mid-ship cross section. *Naval Arch. & Ocean Engng*. **1984**; 22:200-214.

Smith, C. S.. "Influence of local compressive failure on ultimate longitudinal strength of a ship's hull". *Proceedings 3th Int. Symposium on Practical Design in Shipbuilding*; Tokyo. **1977**: 73-79.

Sun, H. H. and Guedes Soares, C. Reliability-Based Structural Design of Ship-Type FPSO Units. *Journal of Offshore Mechanics and Arctic Engineering*. **2003**; (125):108-113.